

Structure and function of cells in a neural integrator

Ashwin Vishwanathan,¹ Kayvon Daie,³ Alex Ramirez,³
Jeff W Lichtman,⁴ Emre Aksay,³ and H. Sebastian Seung^{1,2}

¹Neuroscience Institute and ²Computer Science Department
Princeton University, Princeton, NJ 08544

³Institute for Computational Biomedicine and
Department of Physiology and Biophysics,
Weill Cornell Medical College, New York, NY 10021

⁴Department of Molecular and Cellular Biology and Center for Brain Science,
Harvard University, Cambridge, MA 02138

April 21, 2016

Abstract

Neural integrators are involved in a variety of sensorimotor and cognitive behaviors. The oculomotor system contains a simple example, a hindbrain neural circuit that takes velocity signals as inputs, and integrates them to control eye position. We combined observations of behavior, physiology, and anatomy to study integrator neurons. Two-photon calcium imaging of the larval zebrafish hindbrain was performed while simultaneously monitoring spontaneous eye movements. Integrator neurons were identified as those cells with activities highly correlated with eye position, and the same neurons were then reconstructed from serial electron microscopic images. Cell bodies in more rostral locations had ipsilaterally projecting axons, identified by the existence of presynaptic boutons containing vesicles. Cell bodies in more caudal locations appeared to have contralaterally projecting axons, identified by a distinctive glial ensheathment near the midline. Cells with both ipsilateral and contralateral projections were also reconstructed. Based on previous reports of correlation between somatic location and neurotransmitter identity, we infer that cells with only ipsilaterally projecting axons are largely glutamatergic and excitatory, whereas cells with only contralaterally projecting axons are largely GABAergic and inhibitory. We observed the first conclusive evidence of synapses between integrator neurons, from an ipsilaterally projecting cell onto other cells.

1 Introduction

The larval zebrafish has become an important model organism for investigating the relation between neural circuits and behavior [Friedrich et al., 2010]. Neural activity has been observed via two-photon calcium imaging and correlated with a variety of behaviors [Ahrens et al., 2012]. Here we extend this approach by combining two-photon calcium imaging of neurons in a behaving fish with subsequent reconstructions of the same neurons using serial electron microscopy. The behavior is spontaneous eye movements, and the neurons are in a hindbrain neural circuit known as the "velocity-to-position neural integrator," or "neural integrator" for short [Major and Tank, 2004, Joshua and Lisberger, 2015].

Integrator cells are operationally defined as premotor neurons that carry a horizontal eye position signal in their spiking. (There is also an integrator for vertical eye movements, but it will not be discussed here.) Integrator cells are thought to send their eye position signals through direct synapses onto extraocular motor neurons in the ipsilateral abducens nucleus. They are also thought to receive signals from multiple convergent pathways that encode eye velocity for every type of eye movement. Therefore, the neural integrator is the "final common pathway" for all types of eye movements in fish [Pastor et al., 1994, Aksay et al., 2000, 2001], rodents [van Alphen et al., 2001], non-human primates [Robinson, 1989, Newcombe, 2008], and humans [Leigh and Zee, 2015]. The neural integrator gets its name

because the transformation of eye velocity into eye position is the computational operation of integration with respect to time.

The mechanisms supporting temporal integration remain unclear even after decades of research . Many hypotheses and models have been proposed, and a number of them depend on assumptions about the structure of the underlying neural circuit [Kamath and Keller, 1976, Arnold and Robinson, 1997, Seung, 1998, Seung et al., 2000, Goldman, 2009, Fisher et al., 2013]. Testing these assumptions requires studies that correlate structure and function of integrator neurons.

Structure-function studies were previously performed by two methods. The first relied on intracellular recording to identify goldfish hindbrain neurons exhibiting spiking correlated with eye position [Aksay et al., 2000]. Dye was injected into these cells, which were then reconstructed. The second method relied on two-photon calcium imaging to identify zebrafish integrator neurons with eye position signals [Lee et al., 2015]. These were targeted for single cell electroporation of a fluorescent indicator and reconstructed. Both of these studies relied on light microscopy for structural information. As a result, they were limited to one or a few neurons in any individual brain, and could not positively identify synapses. They could not conclusively distinguish between axon and dendrite, nor could they examine connectivity between integrator neurons. This paper applies serial section electron microscopy (EM) to yield improved structural information about many integrator neurons from a single animal.

Integrator neurons were identified in the hindbrain of a larval zebrafish using two-photon calcium imaging while recording spontaneous eye movements. The same region of the hindbrain was then imaged via serial section electron microscopy. Analysis of the calcium data identified 22 integrator neurons, defined by neural activities that were highly correlated with eye position. The same neurons were located in the EM dataset, and their neurites were completely reconstructed within the confines of the imaged volume.

We identified chemical synapses in our images by the existence of presynaptic vesicles and postsynaptic densities. All chemical synapses involving integrator neurons contained small vesicles, suggesting the presence of conventional rather than peptidergic neurotransmitters. Dense core vesicles were found at other synapses in the same region.

We found 6 integrator neurons with only ipsilaterally projecting axons, identified by the existence of presynaptic boutons containing vesicles. We found 8 integrator neurons with only contralaterally projecting axons, identified by a distinctive glial ensheathment near the midline. Both axonal projection patterns are consistent with a previous report based on light microscopy [Lee et al., 2015]. In addition, we found two integrator neurons with axonal arbors that were both ipsilateral and contralateral, which has not been previously reported. For 6 integrator neurons, an axon could not be identified, presumably because it was cut off by the boundary of the imaged volume.

We found one example of an ipsilaterally-projecting integrator neuron that made two synapses onto another ipsilaterally-projecting integrator neuron. The same source neuron also synapsed onto two contralaterally-projecting integrator neurons. This provides the first evidence that integrator neurons make synapses onto each other.

The neuronal cell bodies in this region are organized into “stripes,” and previous studies have shown that cell body location relative to these stripes is correlated with neurotransmitter identity [Higashijima et al., 2004, Kinkhabwala et al., 2011, Koyama et al., 2011]. On this basis, we inferred that integrator neurons with only ipsilaterally projecting axons are glutamatergic, and those with only contralaterally projecting axons are GABAergic.

We note that two-photon calcium imaging and serial electron microscopy have been successfully combined in the mouse retina [Briggman et al., 2011] and primary visual cortex [Bock et al., 2011, Lee et al., 2016]. Our work is the first application of this approach to a population of neurons defined by their encoding of behavioral variables, rather than stimulus variables.

2 Results

2.1 Identification of integrator cells by two-photon calcium imaging

Calcium signals were correlated with eye position to identify integrator somata from the imaged planes (Fig. 1A) [Miri et al., 2011]. If saccade-triggered average fluorescence was correlated strongly with saccade-triggered eye position (Pearson coefficient > 0.6), the cell was identified as an integrator neuron (Fig. 1A, c). These cells have distinct, graded persistent firing during eye fixation, as seen by the decay time constants of firing during fixation. Average saccade triggered responses of these cells show cells with a range of persistence times. Cells with high persistence had long calcium decay time constants, whereas leaky cells had shorter decay time constants (Fig. 1A, b). This resulted in the identification of 22 integrator cells from 3 distinct imaging planes that were $10 \mu\text{m}$ apart.

Following functional imaging, we imaged the entire hindbrain of the animal with optical sections that were $1\text{ }\mu\text{m}$ apart, producing a light microscopic volume (LM volume) (Fig. 1A, d). The region of interest was then imaged by serial section electron microscopy (Fig. 1B and Methods), resulting in an EM volume. The LM and EM volumes were registered to each other, producing good correspondence of labeled cells and blood vessels (Fig. 1C). All 22 integrator cells from the LM volume were located in the EM volume (Fig 1D).

2.2 General anatomical properties

The EM volume contained a total of 2967 somata spread over rhombomeres 5 through 8. The volume also contained well-known landmarks like the Mauthner cell [Lee et al., 1993], the axon of the contralateral Mauthner cell, cells MiD2 and MiD3 of the reticulo-spinal network [Lee et al., 1993], and a number of commissural bundles (Fig. 1D).

Somata

The somata of the 22 integrator cells spanned $23\text{ }\mu\text{m}$ in the dorsoventral axis and the entire rostrocaudal extent of the imaged volume. The soma locations ended up in three broad clusters. The first cluster of cells was located very close to the midline and at the rostral end of the imaged volume. The second cluster of cells was located at the caudal end of the imaged volume, lateral to the first cluster. A third loose cluster of cells was located at the lateral end of the volume, with cells that spanned the entire rostrocaudal range (Fig. 1D). The average diameter of somata was $4.5 \pm 0.6\text{ }\mu\text{m}$ (mean \pm standard deviation). On average 3.3 ± 1.5 neurites emerged from the somata, and traveled ventrally. Some neurites exited the imaged volume, leading to incompletely reconstructed cells. On average, fully reconstructed cells had total neurite length of $832 \pm 269\text{ }\mu\text{m}$.

Synapses

We identified synapses by the presence of a presynaptic vesicle pool and an opposing postsynaptic density (Fig. 2B, EM panels). Synapses from or onto integrator neurons contained small vesicles, presumably containing a conventional neurotransmitter. Elsewhere in the volume we did identify synapses with dense core vesicles, presumably containing a peptide neurotransmitter (Sup. Fig. 1).

The postsynaptic densities were observed as a darkening of the membrane, indicative of more electron dense regions (Fig. 2B). The presynaptic site was generally at a varicosity in the axon with vesicles throughout. Opposing the postsynaptic density, a small, denser cluster of vesicles was typically observed, along with a presynaptic density. These features are consistent with the idea of a presynaptic active zone.

In total, we annotated 406 presynaptic and 2229 postsynaptic sites on integrator neurons. The number of postsynaptic sites on a cell averaged 101 ± 74 . This is a reasonable estimate of the number of input synapses to an integrator neuron, because most dendritic arbors were reconstructed in their entirety. The number of presynaptic sites on a cell averaged 58 ± 44.39 . This is an underestimate of the number of output synapses from an integrator neuron, because most axonal arbors were cut off by the borders of the volume. If statistics are restricted to the 3 cells that were more complete than others, there were 156 ± 47.46 postsynaptic sites and 97 ± 38 presynaptic sites.

Along the somatic membrane, a darkening of the membrane interrupted by small gaps was often observed (Sup. Fig. 2). The darkening persisted over multiple serial sections, suggesting that it was not an artifact of tissue preparation or imaging. We speculate that these darkenings are electrical synapses, which are known to exist in the developing larval zebrafish hindbrain [Jabeen and Thirumalai, 2013]. We cannot be sure of our interpretation because of our limited image resolution.

Dendrites

Dendrites were defined by the absence of presynaptic vesicles and the presence of postsynaptic densities. They were mostly oriented along the mediolateral axis, but some exceptions were oriented rostrocaudally. Dendrites were smooth rather than spiny (Fig. 2 A-D). The dendritic arbors of these cells fell into a distribution with a long tail, see distribution of arbor size (Sup. Fig. 3). Cells with small arbors were completely reconstructed and did not have any dendrites that left the imaged volume.

Axons

We defined axons as neurites with presynaptic vesicles. No axons were observed emerging directly from the cell body. Instead, dendrites bearing postsynaptic sites turned into axons with presynaptic sites. Two example dendrite-axon transitions are indicated in Fig. 2A and B (open arrow). The main trunk of the axon extended rostrally and ventrally (Fig. 2 A,B,C). From the main trunk emerged mediolateral branches, which we will term collaterals. Those at the rostral extreme of the volume appeared to overlap with the expected location of the abducens motor nucleus (based on its known position within rhombomere r5,6) . In total, we reconstructed 1.62 mm of axonal length in the imaged volume.

We observed dark sheaths around some axonal segments. In some locations, we saw evidence that the sheath wrapped around the axon multiple times (Fig. 2A, EM panel), so we inferred that the sheaths were myelination. The axon of the cell in Fig. 2A was intermittently myelinated along its rostrocaudal section. Mediolateral collaterals emerged from the gaps in myelination, and remained unmyelinated. Myelin sheaths have been previously seen in larval zebrafish spinal cord and wrap neurons in an activity-dependent manner [Mensch et al., 2015, Hines et al., 2015].

Caliber of neurites

In contrast to the current work, previous light microscopic reconstructions of integrator cells [Lee et al., 2015] could not visualize synapses, and therefore inferred whether neurites were axons or dendrites. To investigate the reliability of such inferences, we quantified the caliber of our axons and dendrites. For 20 out of 22 cells, the mean axonal diameter was less than the mean dendrite diameter, conforming to the textbook notion that axons are thinner than dendrites (Fig. 3H). However, the axon was thicker than the dendrites for the remaining two cells, so inference of neurite identity based on caliber would have been erroneous for these cells. Furthermore, neurite diameters are close to the diffraction limit, so that light microscopic estimation of dendritic diameters could be inaccurate.

Small protuberances

A small fraction (3% or 89/2229) of the postsynaptic sites were located on finger-like projections from dendrites that were enveloped by invaginations of axonal boutons (Fig. 2B, EM panel 2). These projections resemble structures found across multiple species called spinules, and are thought to be present on large, active synapses [Petrilia et al., 2015]

Another interesting feature observed on all integrator cells was a short (typically $< 1 \mu\text{m}$) neurite enriched with microtubules emerging from the cell body. In some cases, the neurite terminated inside processes that were presumed glial (Fig. 2D, Sup. Fig. 4).

Putative axons

We noticed that a few of the neurites that crossed the midline shared common features. First, these neurites were devoid of any pre- or postsynaptic sites. Second, before crossing the midline, the neurite became engulfed by processes that appeared glial in nature (Fig. 2 C,D). These features are typical of axons. The glial engulfment is consistent with the idea of glial bridges that are instrumental in axonal guidance during development [Barresi et al., 2005]. The lack of presynaptic sites is similar to some of the initial segments of the ipsilaterally projecting axons, where there were no presynaptic terminals in the early part of the axon, and presynaptic sites emerged only later on. Finally, the diameter of these neurites were similar to the diameters of ipsilaterally projecting axons (Sup. Fig. 5). We therefore infer that these neurites are contralaterally projecting axons.

Spacing between synapses

We computed the intersynaptic distance for all pre- and postsynaptic sites. The mean distance between synapses on dendrites was $1.69 \pm 1.8 \mu\text{m}$ and on axons was $1.93 \pm 3 \mu\text{m}$. However, we noticed that at the level of the individual cell, there were some differences that were not being captured by lumping all cells together. Therefore we broke the distribution of the intersynaptic distance by groups (addressed later). We noticed that for cells in ipsi-only group, the inter presynaptic distances had a long tail, with large gaps. This was indicative of the clustering of presynaptic sites that was visible in (Fig. 2B, graphic inset)

2.3 Axonal projection patterns

We divided the reconstructed integrator cells into four groups based on their axonal arbors, as described below.

*Ipsilateral projection only (“*ipsi-only*”)* - Six cells were observed to have only ipsilaterally projecting axons. Two representatives are shown in Figs. 2A and B. The axons were clearly identified by the presence of *en passant* boutons with presynaptic vesicles. The cell bodies were located at the rostral extent of the volume, and close to the midline (Fig. 3A, *ipsi-only*). Not all cells in this group had rostral axonal terminations in the abducens nuclei. In fact, only two of these cells terminated near the abducens, although the axons that were incompletely reconstructed projected rostrally, they could potentially terminate in the abducens. The average length of all the axons from all ipsilaterally projecting cells was $270 \pm 244 \mu\text{m}$ with the longest reconstructed axon being $683 \mu\text{m}$. The mean diameter of the axons from these cells averaged $0.21 \pm 0.15 \mu\text{m}$ (Fig. 3B).

Dendrites emerged laterally from somata and always extended ventrally. In one case dendrites were observed to cross the midline, as indicated by the presence of postsynaptic sites (Fig. 3A, *ipsi only*, arrowhead). The average volume encompassed by the dendrites of these cells (convex hull volume) was $3.04 \pm 1.5 \times 10^4 \mu\text{m}^3$. The dendrites in this group arborized over 13.3% of the total imaged volume (Sup. Fig. 4). The average length of dendrites from this group of cells was $391.83 \pm 65.83 \mu\text{m}$. The dendritic arbors were more dense at ventral locations with peak arborization at a depth of $35.6 \pm 8.4 \mu\text{m}$ ventral to the cells somata (Sup. Fig. 6). The mean dendritic diameter averaged to $0.25 \pm 0.15 \mu\text{m}$, which was significantly larger to the axonal diameter (Fig. 3B, $p < 2 \times 10^{-3}$, ttest). On average, cells in this group contained 174.83 ± 88.09 postsynaptic sites, and 56.5 ± 52.75 presynaptic sites (Fig. 3C). Cells tend have postsynaptic sites proximal to the cell somata, whereas presynaptic sites at least $\sim 150 \mu\text{m}$ away from the cell somata. To assess the degree of completeness of the cells that were reconstructed, we compared the EM reconstructions of the cells with the long-range axons to previously reported LM reconstructions of similar neurons (Lee et al. [2015]). We did not observe any significant difference in the total number of axonal collaterals and the length of these collaterals (Sup. Fig. 7).

*Both ipsi- and contralateral projections (“*ipsi-contra*”)* - Two cells had axons with both ipsilateral and contralateral projections (Fig. 2C). Integrator cells from this group were located more lateral to the cells from *ipsi-only group*. The ipsilateral projections resembled the axons of *ipsi-only* group cells (Fig. 3A, *ipsi-contra*). In both cells, another neurite crossed the midline. We infer that this neurite is a contralaterally projecting axon. This cannot be confirmed with certainty, because its presynaptic sites are on the contralateral side of the hindbrain, outside the imaged volume. Our inference is based on a number of cues as mentioned previously. The putative contralaterally projecting axon emerged directly from the soma in one cell, and branched from the ipsilaterally projecting axon in the other cell. In both cases, the midline cross-over happened at locations that were ventral to the cells somata. The average length of the axons in this group was $277 \pm 22 \mu\text{m}$ which was similar to the length of the axons from *ipsi-only group*. Similarly, the dendrites of the cells in the group had an average length of $419.3 \pm 178 \mu\text{m}$. Dendrites from these cells on average occupied $2.9 \pm 2.6 \times 10^4 \mu\text{m}^3$, made up 4.3% of the total volume (Sup. Fig. 4). The mean diameter of the axons from this group averaged $0.2 \pm 0.11 \mu\text{m}$ and that of dendrites was $0.21 \pm 0.12 \mu\text{m}$ (Fig. 3B). These neurons on average had 126.5 ± 70 postsynaptic sites, and 33.5 ± 7.77 presynaptic sites on the ipsilateral side (Fig. 3C).

*Contralateral projection only (“*contra-only*”)* - Eight cells from this group, located at the caudal most extent of the imaged volume, contained exclusively contralaterally projecting putative axons (Fig. 3A, *contra only*). Unlike the previous groups of cells, the axons of these cells almost always (one exception) emerged from the somata of the cell, and crossed the midline at locations ventral to the cells somata, with an average diameter of $0.16 \pm 0.08 \mu\text{m}$. In one case we noticed collateral along the putative axon on the ipsilateral side. This however contained only postsynaptic sites, and was dendritic (Fig. 3A, *contra only*, arrowhead). The average dendritic length was $292.41 \pm 69.75 \mu\text{m}$, and they occupied an average volume of $1.2 \pm 1.3 \times 10^4 \mu\text{m}^3$, which was 7.2% of the total volume. This was significantly shorter as compared the dendrites from *ipsi-only group* and *ipsi-contra group* combined ($p < 0.01$, ttest). Similarly the arbor volume of these dendrites was $7.6 \pm 1.9 \times 10^3 \mu\text{m}^3$, which was significantly smaller than the dendritic arbors of *ipsi-only group*, *ipsi-contra group* combined (Sup. Fig. 4, $p < 0.003$, ttest). On average, these cells received 85.2 ± 39.5 postsynaptic sites (Fig. 3C). The average diameter of dendrites was $0.22 \pm 0.12 \mu\text{m}$; this was significantly larger than the diameter of the axons (Fig. 3B, $p < 2 \times 10^{-6}$, ttest)

*Projection unknown (“*unknown*”)* - The last seven cells were located at the lateral most extent of the volume. For these cells we did not find any neurites with presynaptic sites nor did they have any putative axon (Fig. 3A, *unknown*). We believe this is most likely because these cells were not fully represented in the imaged volume and neurites of these cells exit the volume before the axon was located. The average length of the dendrites for cells from this group was $221.47 \pm 48.70 \mu\text{m}$, and they occupied on average a volume of $1.13 \pm 1.2 \times 10^4 \mu\text{m}^3$, which corresponded to 4.9% of

the total volume (Sup. Fig. 4). These cells on average had 40.83 ± 25.11 postsynaptic sites (Fig. 3C).

2.4 Connectivity between integrator neurons

Many theories of the neural integrator are based on assumed patterns of synaptic connectivity between integrator neurons. For example, it has been proposed that integration is supported by recurrent excitation between neurons on the same side of the brain [Kamath and Keller, 1976, Seung, 1996, Seung et al., 2000, Fisher et al., 2013], and/or mutual inhibition between populations on opposite sides of the brain [Cannon et al., 1983, Arnold and Robinson, 1997, Aksay et al., 2007, Fisher et al., 2013]. The existence of synapses between integrator neurons has been presumed possible, because axon collaterals on integrator neurons have been observed in larval zebrafish [Lee et al., 2015], goldfish [Pastor et al., 1994, Aksay et al., 2000], cats [McCrea and Baker, 1985] and nonhuman primates [Steiger and Büttner-Ennever, 1979]. Such collaterals could potentially contact dendrites of other integrator neurons, but conclusive evidence for contact and synapses has been lacking.

From the axon collaterals of one integrator cell, we found the hypothesized synapses onto other integrator cells. This single cell belonged to the *ipsi-only* group. It made 2 synapses onto another *ipsi-only* cell and 1 synapse each onto two *contra-only* cells (Fig. 4A).

A total of eight cells (*ipsi-only* and *ipsi-contra*) had ipsilaterally projecting axons. Based on this projection pattern, it might appear that all eight cells had the *potential* to make synapses onto other integrator neurons within the confines of the imaged volume. However, this would be overstating the case if the axons failed to even approach dendrites. Therefore we decided to define a “potential synapse” as a location where axon and dendrite approached each other closer than $1 \mu\text{m}$ [Stepanyants and CHKLOVSKII, 2005]. We found 48 potential synapses between integrator cells. Of this set, 40 involved the one cell that made the four real synapses. Therefore this cell seemed exceptional in that it made a disproportionate number of potential synapses as well as all the real synapses. This number dropped substantially if the cell was randomly translated by as little as $5 \mu\text{m}$ from the postsynaptic cell (Sup. Fig. 8).

2.5 Inferring neurotransmitter identity

We did not attempt to classify synapses as either symmetric or asymmetric, as there exists some disagreements regarding this method of inference [Klemann and Roubos, 2011]. Instead we attempted to infer neurotransmitter identity based on somatic locations. Cell bodies in the hindbrain of the larval zebrafish follow a stereotypic alternating stripes pattern of cell bodies and neuropil. Cells in the same stripe largely share the same neurotransmitter identity, and morphology [Higashijima et al., 2004, Kinkhabwala et al., 2011, Koyama et al., 2011]. We projected the location of cell somata onto a single plane and noticed the emergence of alternating peaks of cell somata and neuropil, reminiscent of the stripe like pattern. We were able to locate 4 peaks, each corresponding to a likely stripe (Fig. 4C, bottom panel). The medial most peak (Fig. 4C, dotted line) corresponded closely to midline cells from the contralateral population that spilled over in the ipsilateral side imaging, these cells were contralateral to the Mauthner cell axon. Peaks 2-4 were peaks that were visible in the ipsilateral side (the imaged side). Overlaying the 22 integrator somata locations, we noticed that cells in *ipsi-only group* overlapped with peak 2, cells in *ipsi-contra, contra-only group* overlapped with peak 3 and cells in *unknown-group* overlapped with peak4. Based on this, we inferred the putative neurotransmitter identity of the integrator cells. The first stripe on the ipsilateral side (peak2) overlaps with cells that express the *alx* transcription factor, and are mostly glutamatergic [Kimura et al., 2006]. This stripe was also previously shown to almost exclusively contain glutamatergic integrator cells [Lee et al., 2015]. The second stripe (peak3) corresponds cells expressing the transcription factor *dbx1b* [Kinkhabwala et al., 2011]. Integrator cells of different neurotransmitter identities have been reported along this stripe. Cell more dorsal are thought to be glutamatergic, and the more ventral ones expressing GABA. The last, most lateral stripe (peak4) corresponds with cells expressing the *barhl* transcription factor, which is thought to be glutamatergic as well [Colombo et al., 2006, Kinkhabwala et al., 2011].

3 Discussion

Our sample of 22 reconstructed cells is a fairly large fraction of the roughly 100 integrator neurons estimated to exist on one side of the larval zebrafish brain [Aksay et al., 2003]. Eight of the reconstructed cells had ipsilaterally projecting axons. Of these, one cell made synapses onto other reconstructed neurons. This may be an underestimate of integrator connectivity, for several reasons. First, there are many cells in the imaged volume that carried no usable

calcium signal at all, largely because they did not take up enough calcium indicator. Some of these cells are likely to be integrator neurons overlooked by our study, and are potential postsynaptic partners of the reconstructed cells in our sample. Second, there are many integrator neurons outside the imaged volume, and they could receive synapses from our reconstructed integrator neurons. (Only three axonal arbors were fully or mostly reconstructed; the rest appeared substantially cut off as their axons left the volume.) Third, we had no possibility of finding connections between neurons on opposite sides of the brain, because only one side of the brain was imaged.

Our work provides the first conclusive evidence for synapses between integrator neurons. This has long been suspected but experimental confirmation has eluded researchers for decades. It is difficult to know whether the single cell that made synapses onto other integrator neurons is an exceptional case, or a representative of a larger population that was incompletely sampled. One intriguing possibility is that the integrator population contains a subset of cells that are well-connected with each other, while the rest mainly make synapses onto neurons outside the integrator. More definitive information about connectivity patterns between integrator cells awaits a future experiment with an imaged volume that is large enough to encompass all integrator cells, and a fluorescent calcium indicator that labels a higher percentage of integrator cells.

4 Experimental procedures

Two-photon calcium imaging. A larval zebrafish (5-6 dpf) was injected with calcium sensitive dye Oregon Green 488 BAPTA-1 (OGB-1, supplier?) by gently removing skin over the hindbrain and using a patch pipette for iontophoresis. The next day the animal was imaged on a custom two-photon microscope (XwavelengthX). The animal was immobilized in low melting agar and was positioned to view a monitor with light gratings. The hindbrain of the animal was imaged at (XwavelengthX) at predefined plane at (Xspeed HzX). Following functional imaging, the animal was then imaged on the same setup for anatomical imaging. Briefly, a stack was acquired over the same imaging window, with optical sections every 1.3 μm , and with a lateral resolution of 0.5 μm . Once this was performed, the animal was anesthetized and the skin over the hindbrain was removed, to facilitate penetration of the fixative, and the animal was immersed in fixative to preserve the ultrastructure. We found that the removal of the skin over the hindbrain was important for good ultrastructure preservation and for even staining of the tissue.

Serial section electron microscopy.

The animal was immersed in a fixative of 1% paraformaldehyde and 1% glutaraldehyde buffered in 0.1M cacodylate buffer for 24 hrs. Then it was thoroughly washed in 0.1M cacodylate buffer before staining. The tissue was stained using a conventional ROTO procedure (Tapia et al. [2012]). Following staining, the tissue was infiltrated with an LX-112 based EPON resin for 24 hrs and baked for 48 hrs at 60 C. The EPON based resin was tailored to be a low viscosity resin to help with better infiltration for this tissue. Following hardening, the tissue block face was coarsely trimmed and a rectangular mesa was defined for serial sectioning. Care was taken to orient the specimen to permit sectioning along the horizontal axis. Serial sections from the above animal were collected approximately from the level of the Mauthner cell at a thickness of 45 nm. The serial sections were collected using the automatic tape-collecting ultramicrotome (ATUM) [Hayworth et al., 2014, Kasthuri et al., 2015]. The serial sections were then adhered to a silicon wafer, using double sided carbon tape (TEDpella), the wafers were coated with a thin film of carbon to make them conductive. Each wafer was imaged in a Zeiss Sigma field emitting scanning electron microscope in the backscattered electron mode using a custom software interface to collect the images (Hayworth et al. [2014]). The imaged volume was $220 \times 112 \times 57 \mu\text{m}^3$. The images were montaged and aligned using the TrakEM2 plugin in FIJI/ImageJ (Cardona et al. [2012]). Briefly, images were imported into the TrakEM2 framework and montaged, first, using affine transforms, followed by elastic transforms. The images were then registered using a similar approach, where the first pass was performed using affine transforms, followed by elastic transforms. All the alignment was performed on a machine with 32 cores and 120GB RAM.

Registration of light and electron microscopic images.

We first identified potential integrator cells from the LM dataset using methods that were previously described (Miri et al. [2011]). Briefly, to locate the same cells that were identified from the functional imaging, the LM volume was registered to the EM volume. This was done using gross anatomical features like easily recognized clusters of cell bodies and blood vessels, that were readily visible in both the LM and the EM volumes. These features served as anatomical landmarks, where each pair of features were marked as a corresponding pair that was subsequently used to generate a transform. Once we had many such corresponding pairs, they were used to generate an affine transform that was used to register the LM volume on the EM volume. This process was also performed in the Fiji plugin TrakEM2

(Cardona et al. [2012]). This process resulted in overlaying the LM volume onto the EM volume. Once this was done, we were able to locate the VPNI cells in the EM volume. Although these cells were from three distinct planes in the light microscopic volume, their locations in the EM volume was not necessarily restricted to three distinct planes, since we annotated the centers of the cells in the EM volume.

4.1 Registration of light microscope and electron microscope volumes

We first performed functional imaging in an awake, immobilized larval zebrafish using the calcium sensitive dye OGB, by introducing the dye in the hindbrain via iontophoresis, similar to methods used previously (Aksay et al. [2007], Miri et al. [2011]). Once this was done, the animal was placed in an imaging setup that allowed for imaging the activity in the hindbrain, while simultaneously imaging the eye movement behavior. This paradigm allows for the correlation of eye movement behavior to the firing of cells in the hindbrain. We performed the functional light microscopy at pre-defined planes close to and below the Mauthner cell (Fig. 1A, a), unilaterally. This landmark would later serve to identify cells in the electron microscopy volume, since the Mauthner cell is immediately visible in EM sections. Following the functional imaging, the volume was imaged for anatomical landmarks, like blood vessels and location of cell bodies, this volume was termed the light microscopy (LM) volume (Fig. 1A, d). We later extracted the locations of cells whose firing had high degree of correlation to eye-position, and had the firing characteristic of neural integrator cells.

Once functional imaging of the larva was performed, it was immediately prepared for electron microscopy by immersing in fixative. The larva was processed for electron microscopy using conventional reduced osmium staining techniques and embedded in an epoxy based resin (Tapia et al. [2012]). The tissue block was then coarsely trimmed until the appearance of the Mauthner cell plane. Following the observation of this landmark, ultra-thin sections (Fig. 1B, 1st panel) were collected in an automated manner using an automated tape collecting ultramicrotome (ATUM) as described previously (Hayworth et al. [2014]). The sections were then made conductive, by evaporating a thin layer of carbon and imaged in a field emitting scanning electron microscope (FE-SEM) to obtain an electron microscopy (EM) volume. Each section was imaged at a resolution of 5nm/pixel in a region of interest that roughly corresponded with area imaged on the light microscopic (Fig. 1B, 2nd panel). The EM volume we imaged contained 15791 image tiles (8K x 8K pixels each) or $\sim 10^{11}$ pixels (Fig. 1B). These images were registered using the trakEM2 plugin in Fiji (Cardona et al. [2012]). Briefly, individual images were first montaged using affine transforms followed by elastic transforms. Following this they were aligned in the z dimension, using first, affine and followed by elastic transforms.

To locate the cells that were involved in the integrator circuit, we first extracted the location of cells in the light microscopic volume that were eye-position sensitive. Once these cells were located in the light microscopic volume, we then needed to register the LM stack to the EM stack in order to locate the same cells in the EM volume. To do this, we made use of the fact that large, gross morphological features should be easy to spot in the EM stack.

Once enough such features were identified, we located these same landmarks in the high-res EM stack. Each pair of landmarks (one from the LM volume and one from the EM volume) was then used to calculate a global affine transform that was applied to transform the LM volume to be overlaid on the EM volume using the TrakEM2 plugin in Fiji (Cardona et al. [2012]). Following this registration, we were able to reliably locate the same cells from the LM and the EM volumes (Fig. 1C).

Reconstructions

The reconstruction of the cells was performed using the TrakEM2 plugin in Fiji/ImageJ. Two expert tracers reconstructed the cells beginning from the cell bodies in an independent manner. During the tracing process, one of the expert tracers annotated all pre and postsynaptic sites for each cell. The skeletonized tree structure was exported from TrakEM2 as *.swc files. These trees were then imported into Matlab using custom scripts to import .swc files and maintain them as trees. The traces of the two tracers were compared by a third reviewer. The third reviewer, independently reviewed points of disagreement and decided which points of disagreement were either over-reconstructed or were under-reconstructed. In some cases, the traces were re-visited by the tracers if it was needed. For the comparison of EM traces with LM traces, the LM traces were traced using the Simple Neurite Tracer (Longair et al. [2011]) plugin in Fiji, and exported as a *.swc file. They were then imported into the same Matlab framework that was used to analyze the EM traces, and used to compute necessary features to compare the LM traces and the EM traces. The total length of all reconstructed neurites in the imaged volume was 9.55 mm. In some cases, the neurite of the cells exited the volume and were thus under-reconstructed.

Analysis

All analysis was performed on Matlab using custom scripts. All traces were exported as .swc files from TrakEM2.

All tree lengths was reported as pathlengths unless noted otherwise. Similarly, all lengths to a pre or post synaptic site was reported as pathlengths. The axon initiation site was annotated as the parent node of the first presynaptic site. For the putative-axons that originated at the soma, they were annotated as beginning from the root node. One cell from ipsi-only group had a putative axon, based on thinness of the axons and the 'bare' initial segment. All neurites that were not axonal were called dendritic. All nodes of the tree were thus divided as axonal nodes or dendritic nodes. Pathlengths were then generated for a tree over all axonal nodes or all dendritic nodes, and the length of the tree was the sum of all axonal length and dendritic length.

The diameter of the trees was generated by drawing a line segment across the cross-section of the tree at a random location along the tree. Many such line segments were drawn across the entire extent of the tree, where the tracer was blinded to the fact whether the neurite was an axon or a dendrite. The measurements were then separated as dendritic diameter or axonal diameter after all the trees were measured in this manner. The values were reported as a mean across all dendritic or axonal measures for a tree. A collateral was defined as all those segments of an axon, that emerged from the central axonal tree. All tree nodes that were axonal were then divided as those that were part of a collateral and those that were not. Following this, pathlengths and numbers were calculated by treating those nodes like any other. The completeness of cells was decided based on the number of neurites that exited the cells.

Arbor densities of the dendrites was computed by projecting all the axonal or dendritic nodes along the desired plane and reported in a normalized scale. Arbor volumes were computed using the Matlab function *convhull*. The statistics for contra-only cells was computed after removing one outlier (Fig. 3C, purple cell) from the analysis. To infer the neurotransmitter identity from the stripe organization of the cell bodies, we annotated the location of all the cell bodies from a low-resolution stack. The cell density was then computed by projecting all the cells along the desired axis. This process picked out the peaks that were visible in the EM images. The location of a stripe was defined as the local peak that emerged from the cell density projecting analysis.

5 Author contributions

Conceptualization, Methodology, and Writing: A.V, E. A., and H.S.S. Formal Analysis: A.V. and H.S.S. Data Curation: A.V. Visualization: A.V. Investigation: K.D performed two-photon calcium imaging. A.V. acquired serial section EM images with assistance from J.W.L., and assembled the resulting image stack. A.R. registered the calcium images with the EM images. A.V. and E. A. reconstructed neurons with help from Ashleigh Showler and A.R. Supervision and Funding Acquisition: E.A. and H.S.S.

6 Acknowledgments

We are grateful to Juan Carlos Tapia, Richard Schalek and Ken Hayworth for assisting us with tissue preparation, the ATUM serial sectioning procedure, and the WaferMapper software for EM imaging. Stefan Saalfeld, Albert Cardona, and Ignacio Arganda-Carreras answered questions about the TrakEM2 plugin for FIJI/ImageJ. Uygar Sümbül assisted with importing skeletons into MATLAB. We thank Heather Sullivan for tissue processing and optimization. We benefited from helpful discussions with David Tank and Kanaka Rajan. HSS acknowledges funding from the Mathers Foundation, Gatsby Foundation, Human Frontier Science Program, NIH/NINDS award 5R01NS076467, and ARO MURI award W911NF-12-1-0594.

References

- Misha B Ahrens, Jennifer M Li, Michael B Orger, Drew N Robson, Alexander F Schier, Florian Engert, and Ruben Portugues. Brain-wide neuronal dynamics during motor adaptation in zebrafish. *Nature*, 485(7399):471–477, May 2012.
- E Aksay, R Baker, H S Seung, and D W Tank. Anatomy and Discharge Properties of Pre-Motor Neurons in the Goldfish Medulla That Have Eye-Position Signals During Fixations. *Journal of Neurophysiology*, 84(2):1035–1049, August 2000.
- E Aksay, G Gamkrelidze, H S Seung, R Baker, and D W Tank. In vivo intracellular recording and perturbation of persistent activity in a neural integrator. *Nature neuroscience*, 4(2):184–193, February 2001.
- Emre Aksay, Robert Baker, H Sebastian Seung, and David W Tank. Correlated discharge among cell pairs within the oculomotor horizontal velocity-to-position integrator. *The Journal of neuroscience : the official journal of the Society for Neuroscience*, 23(34):10852–10858, November 2003.
- Emre Aksay, Itsaso Olasagasti, Brett D Mensh, Robert Baker, Mark S Goldman, and David W Tank. Functional dissection of circuitry in a neural integrator. *Nature neuroscience*, 10(4):494–504, April 2007.
- D B Arnold and D A Robinson. The oculomotor integrator: Testing of a neural network model. *Experimental Brain Research*, 113(1):57–74, 1997.
- Michael J F Barresi, Lara D Hutson, Chi-Bin Chien, and Rolf O Karlstrom. Hedgehog regulated Slit expression determines commissure and glial cell position in the zebrafish forebrain. *Development (Cambridge, England)*, 132(16):3643–3656, August 2005.
- Davi D Bock, Wei-Chung Allen Lee, Aaron M Kerlin, Mark L Andermann, Greg Hood, Arthur W Wetzel, Sergey Yurgenson, Edward R Soucy, Hyon Suk Kim, and R Clay Reid. Network anatomy and in vivo physiology of visual cortical neurons. *Nature*, 471(7337):177–182, March 2011.
- Kevin L Briggman, Moritz Helmstaedter, and Winfried Denk. Wiring specificity in the direction-selectivity circuit of the retina. *Nature*, 471(7337):183–188, March 2011.
- Stephen C Cannon, DAVID A ROBINSON, and Shihab Shamma. A proposed neural network for the integrator of the oculomotor system. *Biological cybernetics*, 49(2):127–136, 1983.
- Albert Cardona, Stephan Saalfeld, Johannes Schindelin, Ignacio Arganda-Carreras, Stephan Preibisch, Mark Longair, Pavel Tomancak, Volker Hartenstein, and Rodney J Douglas. TrakEM2 software for neural circuit reconstruction. *PLoS ONE*, 7(6):e38011, 2012.
- Alicia Colombo, Germán Reig, Marina Miöne, and Miguel L Concha. Zebrafish BarH-like genes define discrete neural domains in the early embryo. *Gene Expression Patterns*, 6(4):347–352, April 2006.
- D Fisher, I Olasagasti, D W Tank, E R F Aksay, and M S Goldman. A modeling framework for deriving the structural and functional architecture of a short-term memory microcircuit. *Neuron*, 79(5):987–1000, 2013.
- Rainer W Friedrich, Gilad A Jacobson, and Peixin Zhu. Circuit Neuroscience in Zebrafish. *Current Biology*, 20(8):R371–R381, April 2010.
- Mark S Goldman. Memory without feedback in a neural network. *Neuron*, 61(4):621–634, February 2009.
- Kenneth J Hayworth, Josh L Morgan, Richard Schalek, Daniel R Berger, David G C Hildebrand, and Jeff W Lichtman. Imaging ATUM ultrathin section libraries with WaferMapper: a multi-scale approach to EM reconstruction of neural circuits. *Frontiers in Neural Circuits*, 8:68, 2014.
- Shin-Ichi Higashijima, Gail Mandel, and Joseph R Fetcho. Distribution of prospective glutamatergic, glycinergic, and GABAergic neurons in embryonic and larval zebrafish. *The Journal of comparative neurology*, 480(1):1–18, November 2004.

Jacob H Hines, Andrew M Ravanelli, Rani Schwindt, Ethan K Scott, and Bruce Appel. Neuronal activity biases axon selection for myelination in vivo. *Nature neuroscience*, 18(5):683–689, May 2015.

Shaista Jabeen and Vatsala Thirumalai. Distribution of the gap junction protein connexin 35 in the central nervous system of developing zebrafish larvae. *Frontiers in Neural Circuits*, 7:91, 2013.

M Joshua and S G Lisberger. A tale of two species: Neural integration in zebrafish and monkeys. *Neuroscience*, 296: 80–91, June 2015.

B Y Kamath and E L Keller. A neurological integrator for the oculomotor control system. *Mathematical Biosciences*, 30(3):341–352, 1976.

Narayanan Kasthuri, Kenneth Jeffrey Hayworth, Daniel Raimund Berger, Richard Lee Schalek, José Angel Conchello, Seymour Knowles-Barley, Dongil Lee, Amelio Vázquez-Reina, Verena Kaynig, Thouis Raymond Jones, Mike Roberts, Josh Lyskowski Morgan, Juan Carlos Tapia, H Sebastian Seung, William Gray Roncal, Joshua Tzvi Vogelstein, Randal Burns, Daniel Lewis Sussman, Carey Eldin Priebe, Hanspeter Pfister, and Jeff William Lichtman. Saturated Reconstruction of a Volume of Neocortex. *Cell*, 162(3):648–661, July 2015.

Yukiko Kimura, Yasushi Okamura, and Shin-Ichi Higashijima. alx, a zebrafish homolog of Chx10, marks ipsilateral descending excitatory interneurons that participate in the regulation of spinal locomotor circuits. *The Journal of neuroscience : the official journal of the Society for Neuroscience*, 26(21):5684–5697, May 2006.

Amina Kinkhabwala, Michael Riley, Minoru Koyama, Joost Monen, Chie Satou, Yukiko Kimura, Shin-Ichi Higashijima, and Joseph Fetcho. A structural and functional ground plan for neurons in the hindbrain of zebrafish. *Proceedings of the National Academy of Sciences of the United States of America*, 108(3):1164–1169, January 2011.

Cornelius J H M Kleemann and Eric W Roubos. The gray area between synapse structure and function-Gray's synapse types I and II revisited. *Synapse*, 65(11):1222–1230, June 2011.

Minoru Koyama, Amina Kinkhabwala, Chie Satou, Shin-Ichi Higashijima, and Joseph Fetcho. Mapping a sensory-motor network onto a structural and functional ground plan in the hindbrain. *Proceedings of the National Academy of Sciences of the United States of America*, 108(3):1170–1175, January 2011.

Melanie M Lee, Aristides B Arrenberg, and Emre R F Aksay. A Structural and Genotypic Scaffold Underlying Temporal Integration. *The journal of neuroscience*, 35(20):7903–7920, May 2015.

R K Lee, R C Eaton, and S j Zottoli. Segmental arrangement of reticulospinal neurons in the goldfish hindbrain. *The Journal of comparative neurology*, 329(4):539–556, March 1993.

WCA Lee, V Bonin, M Reed, B J Graham, and G Hood. Anatomy and function of an excitatory network in the visual cortex. *Nature*, 2016.

R John Leigh and David S Zee. *The Neurology of Eye Movements*. Oxford University Press, USA, June 2015.

Mark H Longair, Dean A Baker, and J Douglas Armstrong. Simple Neurite Tracer: open source software for reconstruction, visualization and analysis of neuronal processes. *Bioinformatics*, 27(17):2453–2454, September 2011.

Guy Major and David Tank. Persistent neural activity: prevalence and mechanisms. *Current opinion in neurobiology*, 14(6):675–684, December 2004.

R A McCrea and R Baker. Cytology and intrinsic organization of the perihypoglossal nuclei in the cat. *The Journal of comparative neurology*, 237(3):360–376, July 1985.

Sigrid Mensch, Marion Baraban, Rafael Almeida, Tim Czopka, Jessica Ausborn, Abdeljabbar El Manira, and David A Lyons. Synaptic vesicle release regulates myelin sheath number of individual oligodendrocytes in vivo. *Nature neuroscience*, 18(5):628–630, May 2015.

Andrew Miri, Kayvon Daie, Rebecca D Burdine, Emre Aksay, and David W Tank. Regression-Based Identification of Behavior-Encoding Neurons During Large-Scale Optical Imaging of Neural Activity at Cellular Resolution. *Journal of Neurophysiology*, 105(2):964–980, February 2011.

Freda Newcombe. Neuropsychology quainterface. *Journal of Clinical and Experimental Neuropsychology*, 7(6):663–681, January 2008.

A M Pastor, R R De la Cruz, and R Baker. Eye position and eye velocity integrators reside in separate brainstem nuclei. *Proceedings of the National Academy of Sciences*, 91(2):807–811, January 1994.

Ronald S Petralia, Ya-Xian Wang, Mark P Mattson, and Pamela J Yao. Structure, Distribution, and Function of Neuronal/Synaptic Spinules and Related Invaginating Projections. *NeuroMolecular Medicine*, 17(3):211–240, May 2015.

D A Robinson. Integrating with neurons. *Annual review of neuroscience*, 1989.

H S Seung. How the brain keeps the eyes still. *Proc. Natl. Acad. Sci. USA*, 93(23):13339–13344, 1996.

H S Seung. Continuous attractors and oculomotor control. *Neural Networks*, 11(7):1253–1258, 1998.

H S Seung, D D Lee, B Y Reis, and D W Tank. Stability of the memory of eye position in a recurrent network of conductance-based model neurons. *Neuron*, 26(1):259–271, 2000.

H J Steiger and J A Büttner-Ennever. Oculomotor nucleus afferents in the monkey demonstrated with horseradish peroxidase. *Brain research*, 160(1):1–15, January 1979.

A Stepanyants and D CHKLOVSKII. Neurogeometry and potential synaptic connectivity. *Trends in neurosciences*, 28(7):387–394, July 2005.

Juan Carlos Tapia, Narayanan Kasthuri, Kenneth J Hayworth, Richard Schalek, Jeff W Lichtman, Stephen J Smith, and JoAnn Buchanan. High-contrast en bloc staining of neuronal tissue for field emission scanning electron microscopy. *Nature Protocols*, 7(2):193–206, February 2012.

A M van Alphen, J S Stahl, and C I De Zeeuw. The dynamic characteristics of the mouse horizontal vestibulo-ocular and optokinetic response. *Brain research*, 890(2):296–305, February 2001.

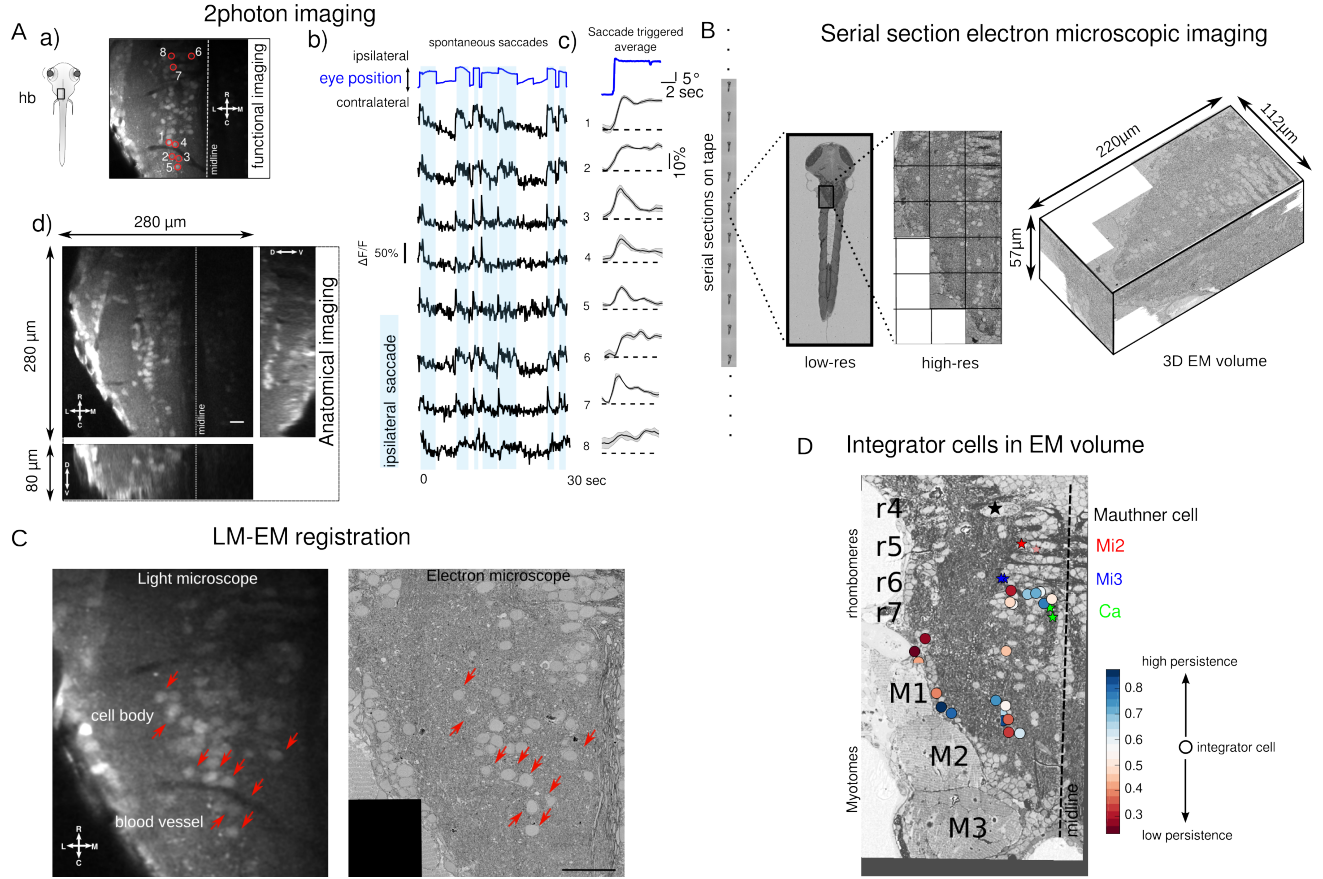


Figure 1: Functional and structural imaging of integrator cells. (A) (a) Larval zebrafish showing the region around which functional imaging was performed (black box) located in the hindbrain (hb). Right panel shows a single imaging plane with cells loaded by calcium indicator OGB-1. Integrator cells identified are shown in red circles. (b) Calcium transients (black traces) from the cell shown circled in (a) to spontaneous saccades (blue trace). Each ipsilateral saccade is highlighted in light-blue. (c) Saccade triggered average of all ipsilateral saccades (blue) with corresponding calcium traces (black) and standard error (grey). (d) Anatomical imaging of the imaged region used to create the light microscopic (LM) volume. Scale bar 20 μm (B) Serial electron microscopy of same zebrafish from A, sections are collected on tape in an automated manner, images at low-resolution are used to align the sections, followed by imaging at high-resolution over the defined region of interest (black box) to give final 3D EM volume of the imaged area. (C) Registration of LM volume to EM volume to locate the cells that were involved in the behavior. Red arrows indicate the same features in both LM and EM. Scale bar 20 μm (D) Anatomical location of all integrator cells (circles) involved in the behavior along with anatomical landmarks, Mauthner cell, Mi2, Mi3 and Ca as identified in the EM volume (stars). Colors of the cells correspond to the persistence time profile of the cell.

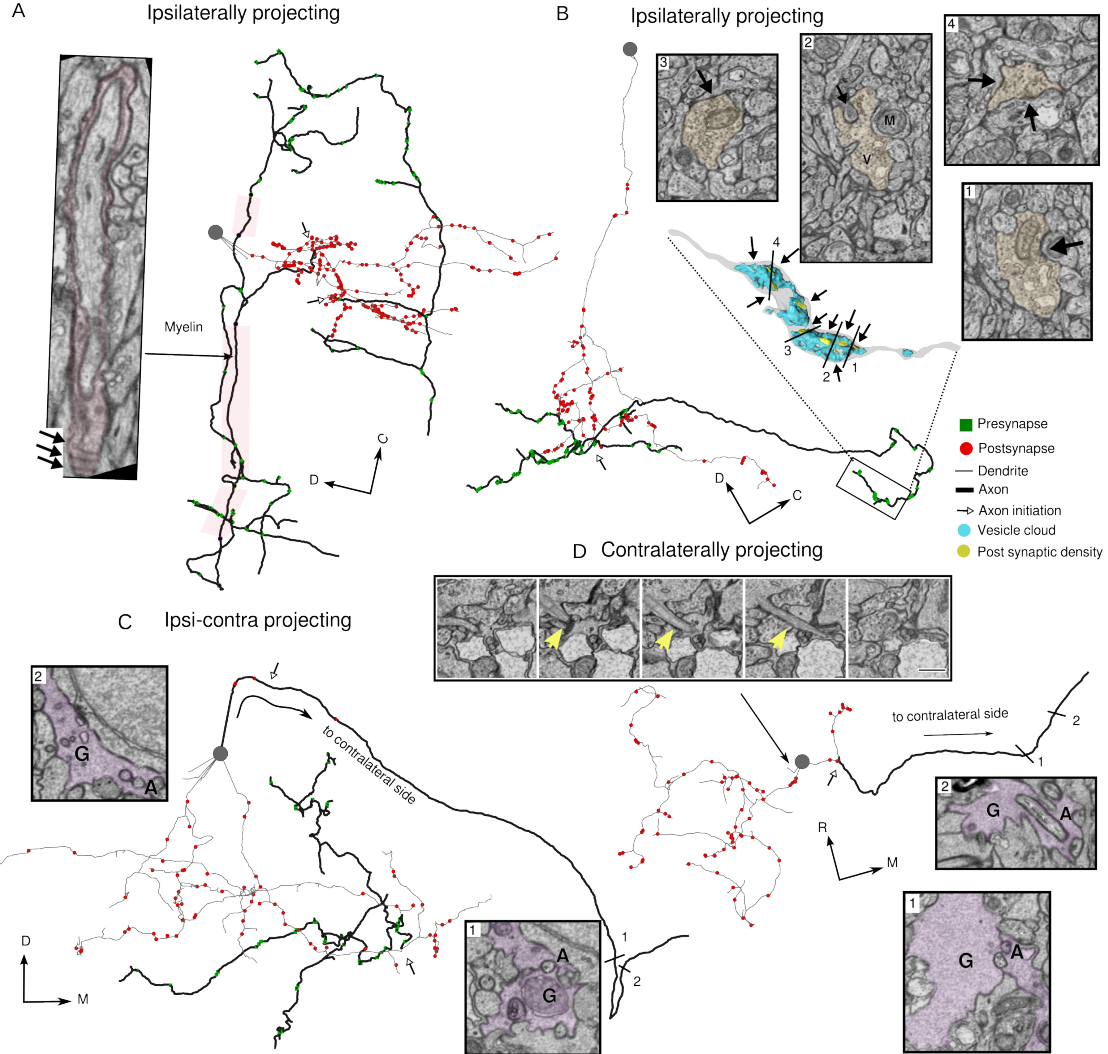


Figure 2: Integrator cell anatomical features reconstructed from EM volume. (A) Example integrator cell showing ipsilaterally projecting axon (dark segment) and dendrite (light segment) with pre- (green) and postsynaptic (red) locations. Parts of the axon of this integrator cell are myelinated (colored boxes). Insets show one such myelinated regions, with arrows showing individual myelin sheaths that are oblique to the imaging plane. Open arrow heads show the location of axon initiation zones along the neurite. (B) Integrator cell, with ipsilateral projecting axon that starts with single neurite that branches to give rise to axon and dendrites. Axon is studded with presynaptic sites that are clustered along neurite. Inset is a 3D reconstruction of axon termination zone with a large vesicle cloud (blue) with multiple post synaptic densities (yellow) opposed to the vesicles. (C) Example integrator cell with both ipsi and contralateral projecting axon. Putative contra axon is engulfed by glial process just before crossing the midline. Inset colored segments are glial G, and non-colored segment is axon A. (D) Contralaterally projecting integrator cell with putative axon crossing the midline with glial engulfment (insets G, A). Also, the somata gives rise to microtubule rich neurite. Shown in large inset panels, the microtubule rich neurite is highlighted with yellow arrow. Note all the integrator somata in this volume give rise to this small neurite, but only one is shown.

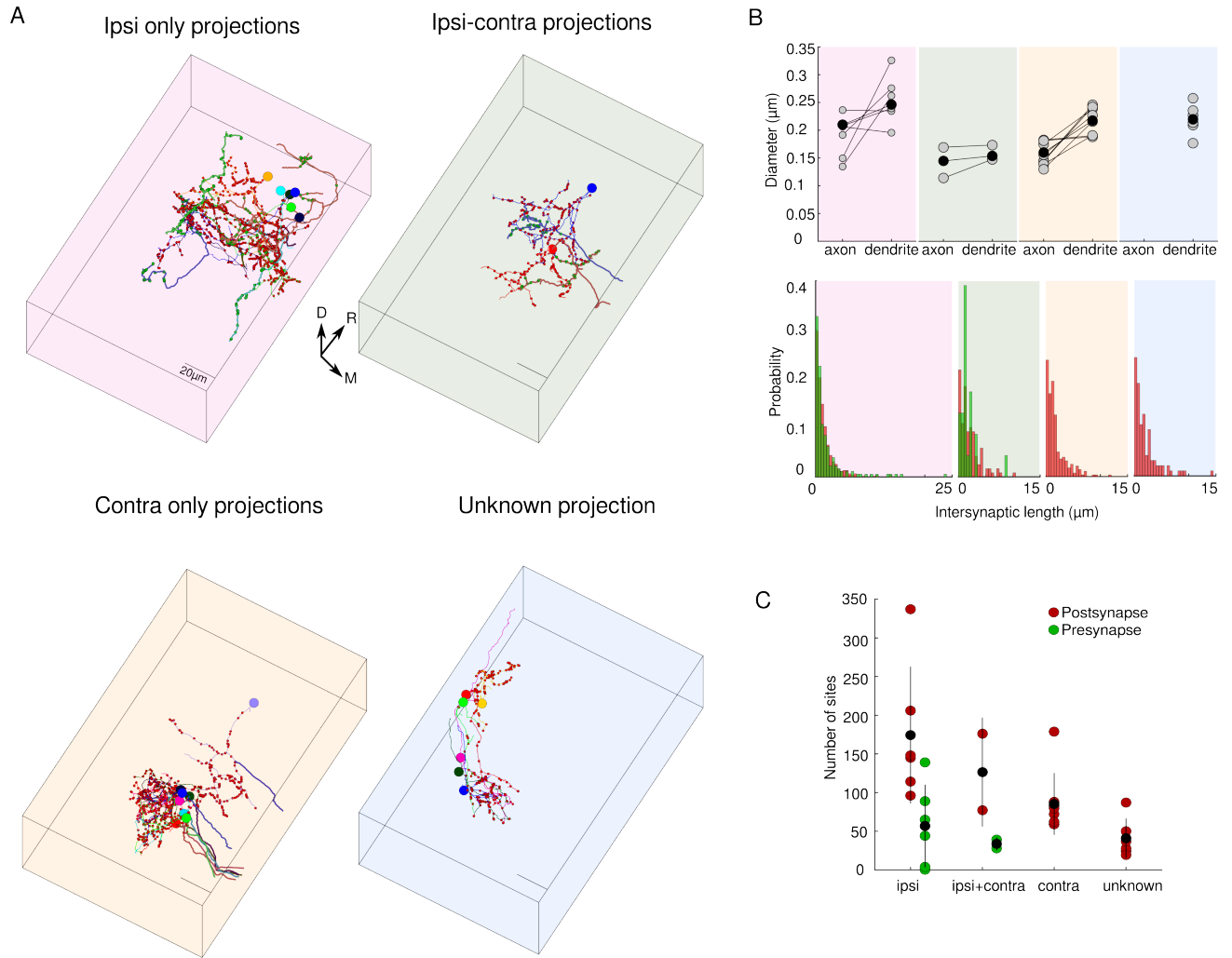


Figure 3: Integrator cells have distinct axonal projection patterns. (A) Top left, 6 integrator cell with ipsilateral projecting axons - ipsi-only group. Top right, 2 integrator cells with ipsilaterally and putative contralateral projection – ipsi-contra. Bottom left, 8 integrator cells with midline crossing contralateral only putative-axon – contra-only. Bottom right, 7, integrator cells with unknown axonal projection – unknown. (B) Upper panel, axonal and dendritic diameter of all cells in each of the four groups. Grey dots are averages for each cell and black dots are averages per group. Lower panel, distribution of intersynaptic distance among pre and postsynaptic sites for all four groups.

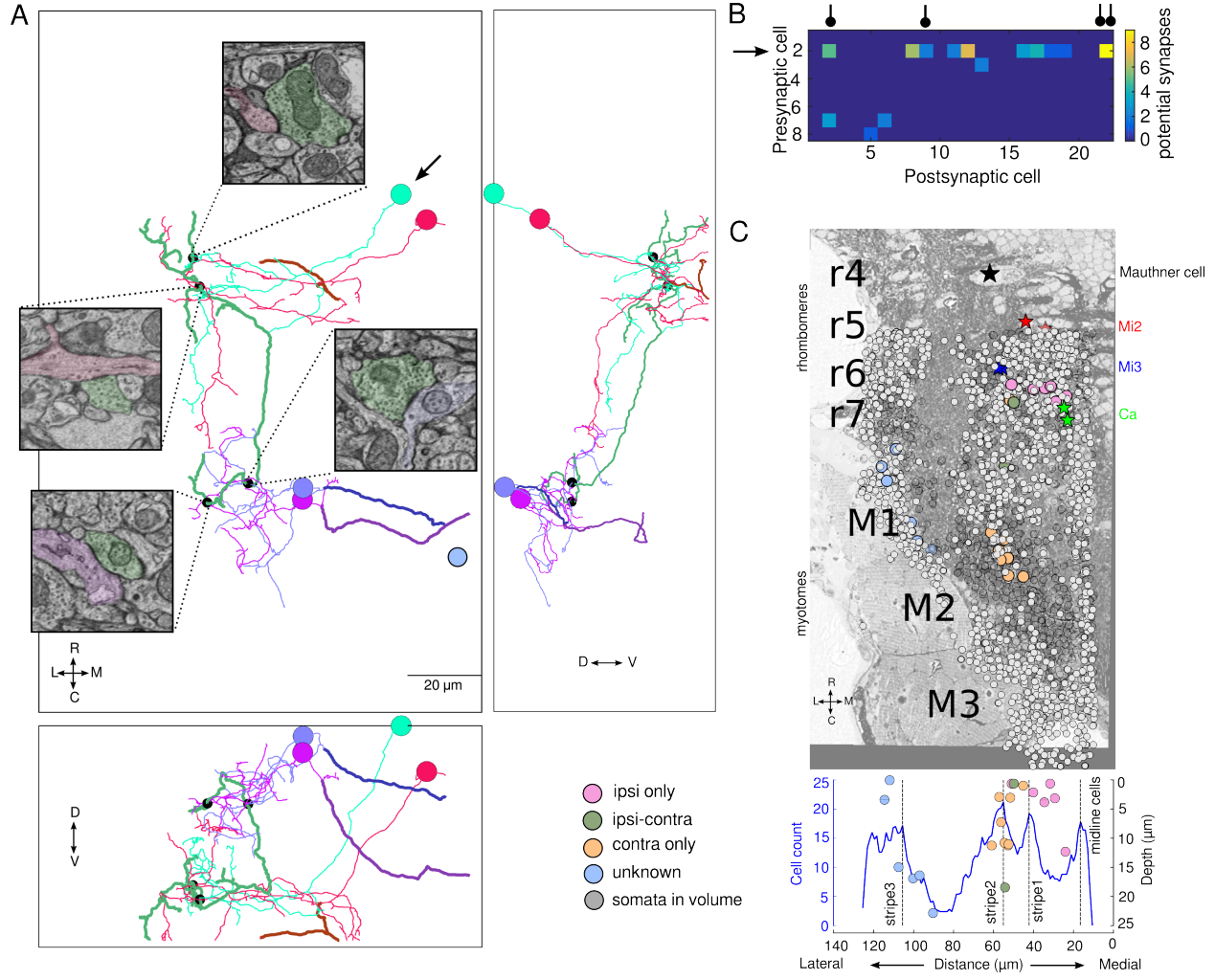


Figure 4: Integrator cell are synaptically connected. (A) Top view of integrator cells that are synaptically connected. All synapses were from one cell (green) in ipsi-only group (arrow) onto one other cell from ipsi-only group (red). One synapses each from ipsi-only group cell (green) onto two contra-only cells (purple and magenta). Black dots represent the site of the synapses, with insets showing the electron micrograph at the respective location. In all electron micrographs, green color is the presynaptic cell, the postsynaptic sites are the same color as the cell somata. Remaining panels are of the same four cells viewed from orthogonal planes. (B) Potential synapse analysis of all sites that are $< 1 \mu\text{m}$ from each other. Cell # 2 (arrow), is the same cell in (A, green) that makes maximum number of potential synapses onto other cells, also makes the real synapses shown in (A). The real synapses are represented by the black circle in the header. (C) Electron micrograph overlaid with identified integrator cells (colored circles), all cells in the imaged volume (grey dots) and anatomical landmarks (colored stars). Lower panel is a distribution of all cells with integrator cells overlaid. Dotted line correspond with hindbrain stripes with known neurotransmitter identities.